Molecular Catalysis 509 (2021) 111629

Contents lists available at ScienceDirect

Molecular Catalysis

journal homepage: www.journals.elsevier.com/molecular-catalysis

In-situ DRIFTS study of chemically etched CeO_2 nanorods supported transition metal oxide catalysts

Yifan Wang, Zhongqi Liu, Matthew P. Confer, Junhao Li, Ruigang Wang *

Department of Metallurgical and Materials Engineering, The University of Alabama, Tuscaloosa, AL 35487, United States

ARTICLE INFO

Keywords:
CeO_2 nanorods
Chemical etching
Surface modification
CO oxidation
DRIFTS
Transition metal oxides

ABSTRACT

In this work, hydrothermally synthesized CeO_2 nanorods (CeO_2NR) were chemically etched by strong reducing agent $NaBH_4$ with 0.6~30 wt% addition, and further transition metal (TM) oxides (TM: Cu, Co, Ni, Fe and Mn) were loaded on the surface modified 6 wt% $NaBH_4$–CeO_2NR powder (mCeO_2NR) to prepare mCeO_2NR supported TM oxide catalysts. Both mCeO_2NR supports (treated by 0.6–30 wt% $NaBH_4$) and mCeO_2NR supported TM oxide catalysts were employed to investigate the effect of chemical etching on their surface structure, CO adsorption, CO_2 desorption and catalytic performance. Compared with pristine CeO_2NR, one strong CO adsorption band for polydentate carbonate is found from *in situ* DRITFS as a result of $NaBH_4$ etching, which can explain the enhanced low temperature reducibility and catalytic performance of mCeO_2NR supports and mCeO_2NR supported TM oxide catalysts. The vibrational band signals of bicarbonate, monodentate/bidentate/polydentate carbonate and bridged carbonate are detected in all mCeO_2NR supported TM catalysts and the effect of CO adsorption mode on CO oxidation activity is discussed.

1. Introduction

Several transition metals (TM) oxides or their mixture, including MnO_x, CuO_x, NiO_x, CoO_x, and FeO_x, have been reported as active, cost-effective and sustainable catalysts to replace costly noble metals (Pt, Rh, and Au etc.) for low-temperature CO oxidation reactions and attracted great attention in recent years [1–5]. Among TM oxide catalysts, copper-containing catalysts or supported copper oxides, including CuO/ZrO_2, CuO/SiO_2, CuO/Al_2O_3 and so on, show superior low-temperature activity and thermal stability [6–9], although the underlying mechanism is not well understood. In order to meet increasing emissions control requirements including EPA regulations challenges, low conversion, poisoning resistance, and thermal stability must be overcome before TM oxide catalysts can be used industrially [10]. It has been reported that TM oxides and reducible oxide supports (CeO_2 and TiO_2) exhibit strong catalyst-support interactions through oxide solid solutions or electronic perturbations, unlike TM oxide catalysts supported on irreducible oxides (ZrO_2, SiO_2, and Al_2O_3) [11,12]. The TM oxide catalysts on reducible oxide supports have demonstrated excellent low temperature activity and are potential candidates to replace noble metal catalysts.

Ceria (CeO_2) is well-known for its excellent oxygen storage capacity and high redox ability via a reversible Ce^{4+} to Ce^{3+} transition [13]. Ceria can act as an active component in many redox-related catalytic reactions and has been extensively studied. CeO_2 nanocrystals with different morphologies, such as nanooctahedra, nanospheres, nanocubes, and nanorods (NR) have been studied to determine the effects of nanoparticle morphology and exposed crystal planes on the activity of CeO_2 supported catalysts [14,15]. According to others' and our previous work [16–18], CeO_2 nanorods (CeO_2NR) supported metals or metal oxides (i.e. Ru and CuO_x) show superior activity in water-gas shift reaction and CO oxidation compared to CeO_2 nanocubes (CeO_2NC) and nanooctahedra (CeO_2NO) supported metals or metal oxides.

In addition to utilization of catalytically active supports, surface modification of supports and catalysts has been widely adopted to further enhance the performance of the existed catalysts system for economic and large-scale practical application [19,20]. For instance, Gao et al. [21] reported that surface engineering of CeO_2NR by chemical redox etching resulted in rough, high porosity catalyst surfaces, which can increase the catalytic activity for CO oxidation due to the enhancement of specific surface area, oxygen vacancy content and the surface Ce^{3+} fraction of CeO_2NR. Furthermore, Bae et al. [22] studied the catalytic activity of nanoscale zero-valent iron (Fe^0) after $NaBH_4$ etching for reduction of p-nitrophenol and found that $NaBH_4$ initiated

* Corresponding author.
E-mail address: rwang@eng.ua.edu (R. Wang).

https://doi.org/10.1016/j.mcat.2021.111629
Received 6 February 2021; Received in revised form 24 April 2021; Accepted 5 May 2021

the disintegration of iron species into smaller clusters with increased reactive surface.

Inspired by our previous results [23], in this study, CeO_2NR was first chemically etched by the strong reducing agent $NaBH_4$ (hereinafter referred to as mCeO_2NR; "m" refers to "modified") and then mCeO_2NR supported 10 wt% TM oxide catalysts were prepared and used to study the effect of chemical etching on low-temperature CO oxidation. *In situ* diffuse reflectance infrared Fourier transform spectroscopy (DRIFTS) was used to elucidate the mechanisms of CO adsorption and oxidation. The effect of strong interactions between TM oxides and mCeO_2NR on CO oxidation is discussed.

2. Experiment

2.1. Preparation of pristine CeO_2NR support

A hydrothermal method was used to synthesize CeO_2NR. According to our previous study [5], 8.8 mmol cerium nitrate hexahydrate ($Ce(NO_3)_3{\cdot}6H_2O$) was dissolved in 88 mL deionized water (DI water) and 48 mmol sodium hydroxide (NaOH) was dissolved in 8 mL of DI water. The NaOH solution was added dropwise into the $Ce(NO_3)_3$ solution with simultaneous mild stirring. After that, the mixture was transferred to a Teflon lined stainless-steel autoclave. After hydrothermal reaction at 90 °C for 48 h, the sample was filtered and dried at 60 °C overnight to obtain the dry, pristine CeO_2NR powder.

2.2. $NaBH_4$ chemical etching treatment of CeO_2NR powder

$NaBH_4$ was used to "modify" the pristine CeO_2NR powder in the following steps. 0.5 g CeO_2NR powder was dispersed in 250 mL of DI water with mild stirring, and 0.6, 3, 6, 12, or 30 wt% $NaBH_4$ was added to the CeO_2NR suspension. The CeO_2NR/$NaBH_4$ suspension was then stirred at room temperature for 12 h. After the solution was filtered and dried at 60 °C overnight, the powder sample was calcined at 300 °C for 5 h in air. Fig. S1 compared the H_2-TPR profiles of mCeO_2NR before and after calcination. After the calcination, the low temperature surface reducibility was significantly improved, which is believed to link with the boron (B) diffusion into the lattice of CeO_2NR during thermal treatment. The samples after calcination were labelled as 0.6, 3, 6, 12, or 30 wt% $NaBH_4$—CeO_2NR. Specially, the 6 wt% $NaBH_4$—CeO_2NR was also noted as mCeO_2NR.

2.3. Deposition of TM oxide catalysts on modified CeO_2NR

The mCeO_2NR powder was used as support to prepare TM oxide catalysts. To prepare supported Cu, Ni, Co, Fe, or Mn catalysts, 0.5 g mCeO_2NR was added to 100 mL DI water with mild magnetic stirring on hot plate, and 10 wt% of TM precursors: $Cu(NO_3)_3{\cdot}2.5\ H_2O$: 98%, from Acros Organics, $NiCl_2$: 98% from Acros Organics, $Co(NO_3)_2{\cdot}6\ H_2O$: 98.0–102.0% from Alfa Aesar, $Fe(NO_3)_3{\cdot}9\ H_2O$: 99+% from Acros Organics and $Mn(CH_3COO)_2$: 98+% from Alfa Aesar were added to the mCeO_2NR suspension. Aqueous ammonia ($NH_3{\cdot}H_2O$) was added dropwise into the TM/mCeO_2NR suspension to control the pH of the samples at ~9. The sample solution was heated to 80 °C for 4 h, filtered and dried at 80 °C overnight. The dry catalyst powders were calcined at 400 °C for 5 h in air to ensure a complete decomposition of TM precursor. The calcined samples were denoted as 10M-mCeO_2NR (*M* = Cu, Ni, Co, Fe, or Mn for each precursor).

2.4. Catalyst characterizations

A Philips X'Pert MPD diffractometer with Cu K α radiation source (λ= 1.5418 Å) was used to obtain the X-ray diffraction (XRD) patterns of the powder samples. The scanning Bragg's angle was set at a range of 2θ from 5° to 90° with scanning rate of 0.01° per second. The working conditions of voltage and current for XRD were 45 kV and 40 mA, respectively.

Transmission electron microscopy (TEM) and scanning transmission electron microscopy (STEM) characterization was conducted using a FEI Tecnai F20 operated at 200 kV, equipped with a high angle annular dark field (HAADF) detector. The samples were dispersed in ethanol and then dropped onto an ultrathin holey carbon film supported on copper grid (from Ted Pella). The energy-dispersive X-Ray spectroscopy (EDS) analysis was employed by the same FEI Tecnai F20 microscope equipped with an EDAX detector to collect EDS spectrum and elemental distributions.

The Brunauer-Emmett-Teller method (BET) was used to determine the specific surface area of the powder samples by measuring N_2 adsorption/desorption at ~ −196 °C through the signal from a thermal conductivity detector (TCD) on the Micromeritics AutoChem II 2920 chemisorption analyzer. The same chemisorption analyzer was also used for hydrogen temperature programmed reduction (H_2-TPR) and carbon monoxide temperature programmed desorption (CO-TPD). The H_2-TPR measurements were operated in a quartz U-tube reactor equipped with a TCD. During the testing, a 10% H_2 /Ar gas mixture (flow rate: 50 mL/min) was introduced and the temperature of reactor with the powder samples (90 mg) was controlled from 30 °C to 900 °C at rate of 10 °C/min. CO-TPD was performed by introducing a 10% CO/He gas flow (flow rate: 50 mL/min) for 1 h at 30 °C first and then heating the samples from 30 °C to 900 °C in a He gas flow (flow rate: 50 mL/min) to monitor the desorption behavior of various gas species. The sample was pre-treated from room temperature to 400 °C under He gas flow to remove residual moisture.

In situ diffuse reflectance infrared spectroscopy (DRIFTS) measurements were studied using a Bruker Vertex 70 FTIR spectrometer equipped with a Harrick DRIFTS cell and measured using a room temperature DLaTGS detector. Before testing, each catalyst was pre-treated inside the cell in UHP N_2 gas environment with a flow rate of 30 mL/min at 200 °C for 30 min to remove the surface moisture. After cooling to 35 °C, the background spectrum was collected at the same flow of N_2. The *in-situ* DRIFTS spectra were collected with 30 mL/min 5 vol.% CO/95 vol.% Ar mixture feeding gas for 40 min, after which the flow was switched back to 30 mL/min UHP N_2 gas for 40 min. During the whole time, the DRIFTS spectra were recorded every 10 min (continuously) by collecting 64 scans with a resolution of 4 cm^{-1}.

2.5. Catalytic activity and stability test

The catalytic stability test for CO conversion was carried out with a fixed bed plug flow reactor system. Typically, 50 mg of catalyst was mixed with quartz wool and loaded into the quartz tube reactor. The sample was heated from room temperature to the experimental temperature (temperature providing ~90% CO conversion) and was kept at that temperature for 24 h under a 1 vol% CO/20 vol% O_2/He gas flow (flow rate: 30 mL/min corresponding to a weight hour space velocity (WHSV) value of 46,000 mL h^{-1} g_{cat}^{-1}). The reactants and products were analyzed by an online gas chromatograph (SRI multiple gas analyzer GC, 8610C chassis) system. The conversion of CO (C_{CO}) were defined according to the following equation:

$$C_{co}(\%) = ([CO]_{in} - [CO]_{out})/[CO]_{in} \times 100$$

Where $[CO]_{in}$ is the influent CO concentration and $[CO]_{out}$ is the effluent CO concentration.

3. Results and discussion

3.1. Morphological and structural characterizations

Part of XRD and Raman data of the CeO_2NR supports after $NaBH_4$ etching and mCeO_2NR supported TM oxide catalysts was reported in our previous work [23]. All the samples containing mCeO_2NR exhibit strong

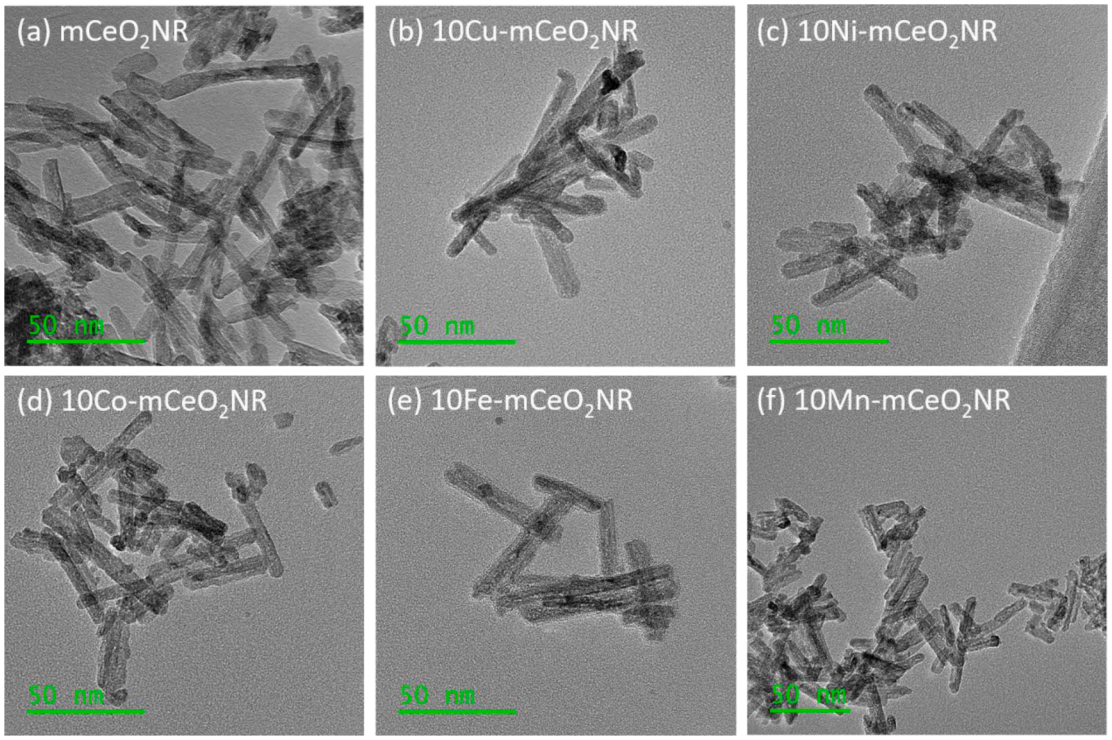

Fig. 1. TEM images of (a) $mCeO_2NR$, (b) 10 Cu-$mCeO_2NR$, (c) 10 Ni-$mCeO_2NR$, (d) 10 Co-$mCeO_2NR$, (e) 10 Fe-$mCeO_2NR$ and (f) 10 Mn-$mCeO_2NR$.

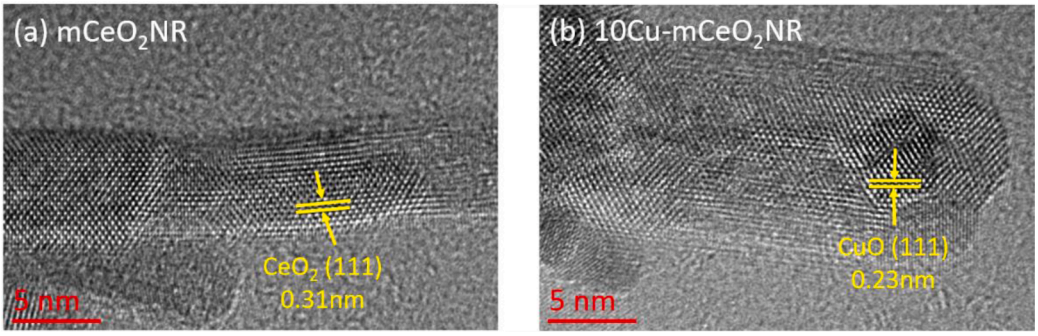

Fig. 2. HRTEM images of (a) $mCeO_2NR$ and (b) 10 Cu-$mCeO_2NR$.

and dominant diffraction peaks related to face-centered cubic fluorite CeO_2 (JCPDS No. 34–0394) with typical Raman signals including triply degenerate F_{2g} vibration near 458 cm^{-1}, doubly degenerate TO vibration near at 255 cm^{-1} and defects-induced band near 600 cm^{-1}.

TEM image of $mCeO_2NR$ (treated by 6 wt% $NaBH_4$), Fig. 1(a), shows that the modified CeO_2NR support is 50–100 nm long and 5–7 nm in diameter. Fig. 1(b-f) contain TEM images of 10 wt% CuO_x, NiO_x, CoO_x, FeO_x, and MnO_x-$mCeO_2NR$ catalysts respectively, and no size or shape change is observed for $mCeO_2NR$ in any of the catalyst samples. HRTEM images of $mCeO_2NR$ and 10Cu-$mCeO_2NR$ are shown in Fig. 2, displaying CuO_x embedded in the lattice of CeO_2NR, which is indicative of strong CuO_x-CeO_2NR interaction. In these supported catalyst samples, the apparent absence of large metal oxide clusters or agglomeration formed or found on the $mCeO_2NR$ support is consistent with the previous results [23], indicating well dispersed TM oxide catalysts on the $mCeO_2NR$ surface or partial diffusion of TM oxides into $mCeO_2NR$ lattice. Fig. S2 and S3 show the STEM images and EDS elemental mapping for 10Cu-$mCeO_2NR$ and 10Co-$mCeO_2NR$, respectively, to identify the copper and cobalt distribution. The EDS mapping results in Fig. S2 and S3 present the excellent distribution of metal species on $mCeO_2NR$.

H_2-TPR profiles of pristine and $NaBH_4$ modified CeO_2NR supports are presented in Fig. 3(a). The results of three samples (0.6/3/6 wt% $NaBH_4$—CeO_2NR) were reported previously and included in Fig. 3(a) for comparison [23]. The H_2-TPR profile of pristine CeO_2NR shows two major hydrogen consumption peaks at 480 °C and 746 °C, which correspond to the surface and bulk reduction of CeO_2 respectively [23]. For $NaBH_4$ modified CeO_2NR supports (0.6, 3, 6, 12, and 30 wt% $NaBH_4$ addition), the onset of hydrogen consumption and surface reduction temperature of $mCeO_2NR$ clearly shifts to lower temperature. H_2-TPR peak shift is especially pronounced for the 6 wt% $NaBH_4$—CeO_2NR sample. The shifted peaks for surface reduction (395 °C for 0.6 wt% $NaBH_4$—CeO_2NR, 394 °C for 3 wt% $NaBH_4$—CeO_2NR, 336 °C for 6 wt% $NaBH_4$—CeO_2NR, 405 °C for 12 wt% $NaBH_4$—CeO_2NR and 401 °C for 30 wt% $NaBH_4$—CeO_2NR) suggest that the addition of $NaBH_4$ significantly

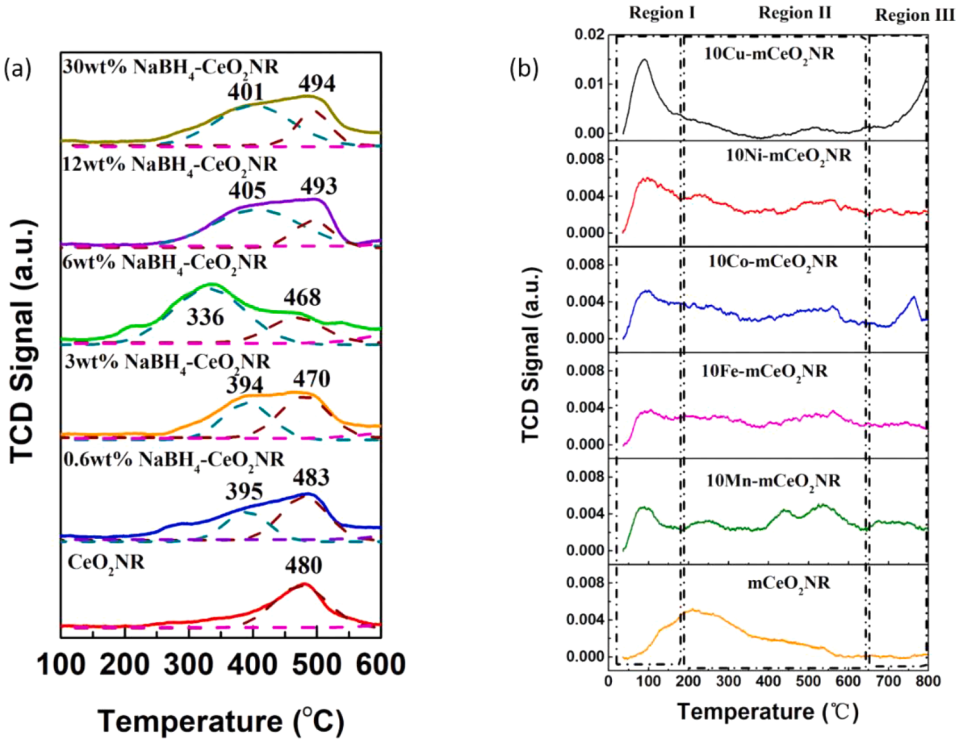

Fig. 3. (a) H_2-TPR profiles of the pristine and modified CeO_2NR supports by 0.6/3/6/12/30 wt% $NaBH_4$ addition (The data for 0.6–6 wt% $NaBH_4$—CeO_2NR samples was reprinted from ref [23]), and (b) CO-TPD profiles for mCeO_2NR supported TM oxide catalysts (It should be noted that the scale of TCD signal for 10 Cu-mCeO_2NR is remarkably larger than others).

Table 1
BET surface area and H_2 consumption of $mCeO_2NR$ with different amounts of $NaBH_4$ addition.

Sample	BET surface area^2/g	H_2 consumption (30 °C to 600 °C) μmol/g	H_2 consumption (600 °C to 900 °C) μmol/g	H_2 consumption (total) μmol/g
CeO_2 NR	120.4	455.8	606.2	1062.0
0.6 wt% $NaBH_4$–CeO_2NR	124.4	741.2	558.2	1299.4
3 wt% $NaBH_4$–CeO_2NR	121.2	740.4	511.1	1251.5
6 wt% $NaBH_4$–CeO_2NR($mCeO_2$ NR)	120.4	1026.2	553.8	1580.0
12 wt% $NaBH_4$–CeO_2NR	114.8	776.9	447.9	1224.8
30 wt% $NaBH_4$–CeO_2NR	98.5	737.6	516.7	1254.3

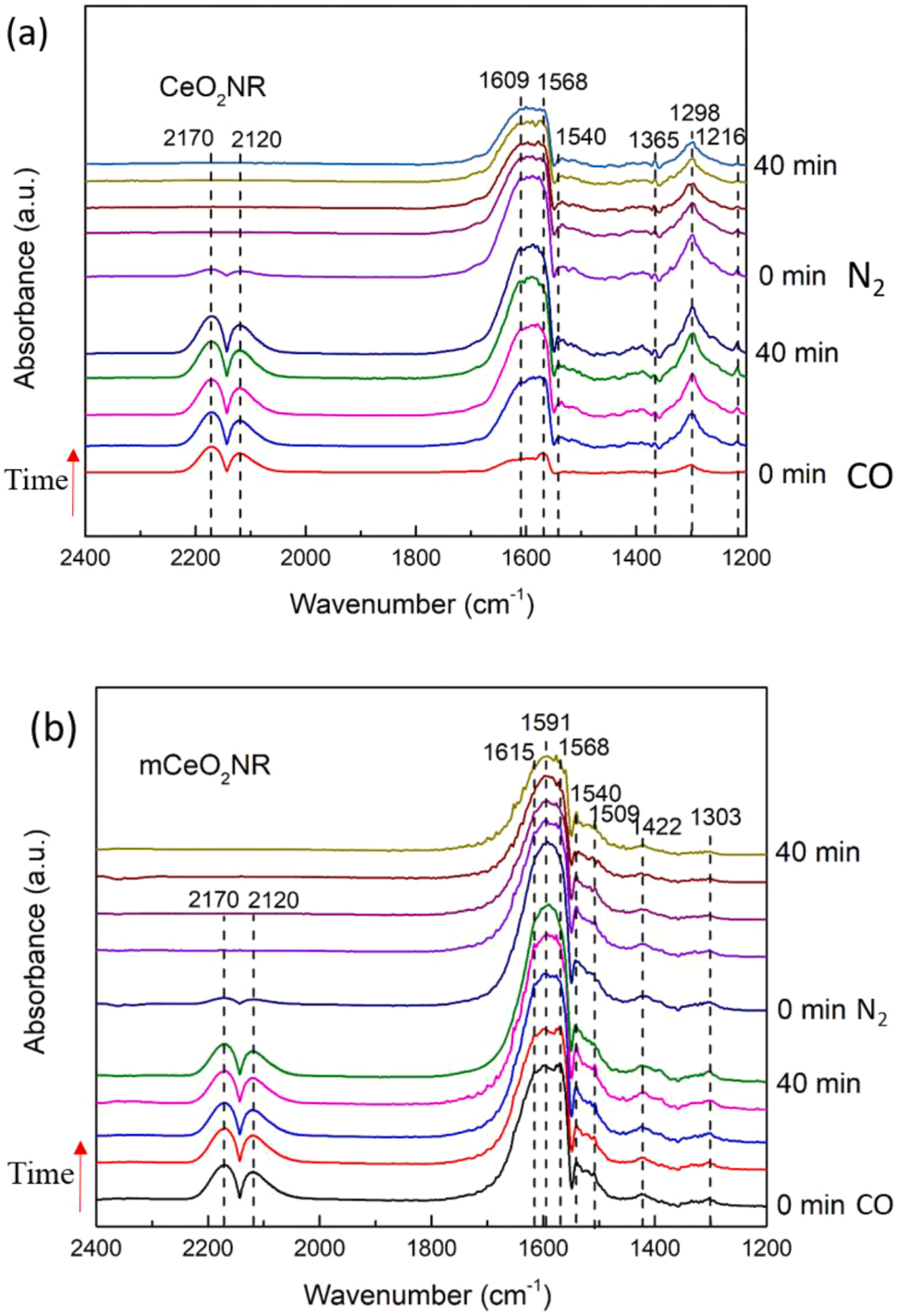

Fig. 4. *In situ* DRIFTS spectra of CO adsorption on (a) pristine CeO_2NR and (b) surface modified CeO_2NR.

Table 2
Peak assignments of *in situ* DRIFTS spectra for CeO_2NR supports before and after $NaBH_4$ etching.

Wavenumber (cm^{-1})	Description	Ref
2170, 2120	CO gas	[31,32]
1609, 1615	bicarbonate	[32,33]
1591	polydentate carbonate 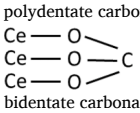	[36,37]
1568, 1303, 1298	bidentate carbonate 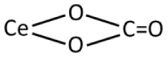	[32,34]
1540, 1509	mono dentate carbonate 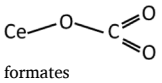	[33,35]
1365	formates 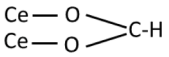	[33,35]
1216	bridged carbonate 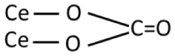	[32,34]
1422	unassigned	

transforms the surface structure and/or chemical composition of CeO_2NR. Combination of H_2-TPR data with previous XPS analysis [23], indicates that the low temperature reduction peaks may be associated with the existence of boron species on mCeO_2NR surface, where boron species might partially involve the surface reduction of CeO_2 NR. Compared to the 6 wt% $NaBH_4$—CeO_2NR, the CeO_2NR supports etched by higher concentrations of $NaBH_4$ (12 and 30 wt%) demonstrate lower BET surface area and higher reduction temperatures, indicating that excess $NaBH_4$ addition inhibits the oxygen release of etched CeO_2NR surface. A possible explanation of the declined reducibility with extra $NaBH_4$ addition is due to the rapid heat release and cluster agglomeration of CeO_2 induced by violent hydrolysis reaction of large amount of $NaBH_4$. The total H_2 consumption of pristine CeO_2NR, 0.6, 3, 6, 12, and 30 wt% $NaBH_4$—CeO_2NR, summarized in Table 1, indicates that $NaBH_4$ etching is an effective surface modification method for preparing highly reducible catalyst support possessing both lower reduction temperature and higher hydrogen consumption compared to the pristine sample, where the H_2 consumption from 600 to 900 °C is assigned as the bulk reduction of CeO_2. This observation is especially true for the H_2 consumption at low temperature range (30 °C to 600 °C, which refers to the surface reduction range), where the 6 wt% $NaBH_4$—CeO_2NR sample showed 125% higher consumption than the pristine CeO_2NR. Based on the H_2-TPR performance, 6 wt% $NaBH_4$—CeO_2NR was chosen as the support material (mCeO_2NR) for the study of gas adsorption and desorption, activity stability test, and *in situ* DRIFTS study of mCeO_2NR supported TM oxide catalysts.

3.2. Temperature programmed desorption (TPD)

CO-TPD profiles of mCeO_2NR supported TM oxide catalysts are presented in Fig. 3(b). The CO_2 desorption peaks in the CO-TPD profiles of supported TM oxide catalysts can be divided into three different temperature regions [24–27]. The peak region I, room temperature to 180 °C, was assigned to the CO_2 desorption from CO oxidation over active surface oxygen species, and the peaks in region II, 180 °C to 650 °C, were assigned to the CO_2 desorption from CO oxidation through lattice oxygen species of CeO_2 and the conversion of surface and interface carbonates. The peaks in region III, 650 °C to 800 °C, correspond to the CO_2 desorption from decomposition of carbonate species. It can be observed that all supported TM catalysts show higher desorption intensity in region I than that of mCeO_2NR, indicating the enhanced CO_2 desorption at low temperature region due to TM-CeO_2NR interaction. The order of relative intensities of peak in the region I is 10Cu-mCeO_2NR >> 10Ni-mCeO_2NR > 10Co-mCeO_2NR > 10Mn-mCeO_2NR > 10Fe-m-CeO_2NR. Based upon the CO-TPD profiles, the amount of active reaction sites for CO oxidation over 10Cu-mCeO_2NR surface is significantly higher than for other TM oxides and the CO_2 product can be easily desorbed.

3.3. In situ DRIFTS study

In situ CO adsorption DRIFTS was performed to identify the active species and sites for catalytic oxidation of CO using mCeO_2NR and mCeO_2NR supported TM oxide catalysts. The *in situ* CO adsorption DRIFTS spectra of both pristine CeO_2NR and mCeO_2NR are presented in Fig. 4. As a result of CO gas flow, the bands at *ca* 2170 and 2120 cm^{-1} are assigned to the free gaseous CO in the testing chamber [28]. After 40 mins of CO flow, N_2 flow was started to remove the gas-phase CO and any weakly adsorbed CO species (including physiosorbed species). CO adsorbed at the surface oxygen sites of CeO_2NR to form various surface species, as shown in Fig. 4, including bicarbonate ($\nu(CO_3)$ at 1609 and 1615 cm^{-1}) [29,30], bidentate carbonate ($\nu(CO_3)$ at 1568, 1303 and 1298 cm^{-1}) [29,31], monodentate carbonate ($\nu(CO_3)$ at 1540 and 1509 cm^{-1}), formate (ν(OCO) at 1365 cm^{-1}) [30,32], bridged carbonate ($\nu(CO_3)$ at 1216 cm^{-1}) [29,31] and unassigned carbonate ($\nu(CO_3)$ at 1422 cm^{-1}). There is a strong band at 1591 cm^{-1} in the mCeO_2NR sample spectra, which was attributed to the polydentate carbonate [33]. According to Vayssilov et al. [34], polydentate carbonate associated with CeO_2 only forms in the vicinity of Ce(III) or oxygen vacancies. The formation of polydentate carbonate species is consistent with our previous results of the XPS analysis for the same sample [35] because mCeO_2NR has a higher concentration of Ce(III) and oxygen vacancies than the pristine CeO_2NR sample. The DRIFTS band assignments of CeO_2NR supports before and after $NaBH_4$ etching are summarized in Table 2.

Notably, shown in Fig. 5, when the CO flow was started to purge into

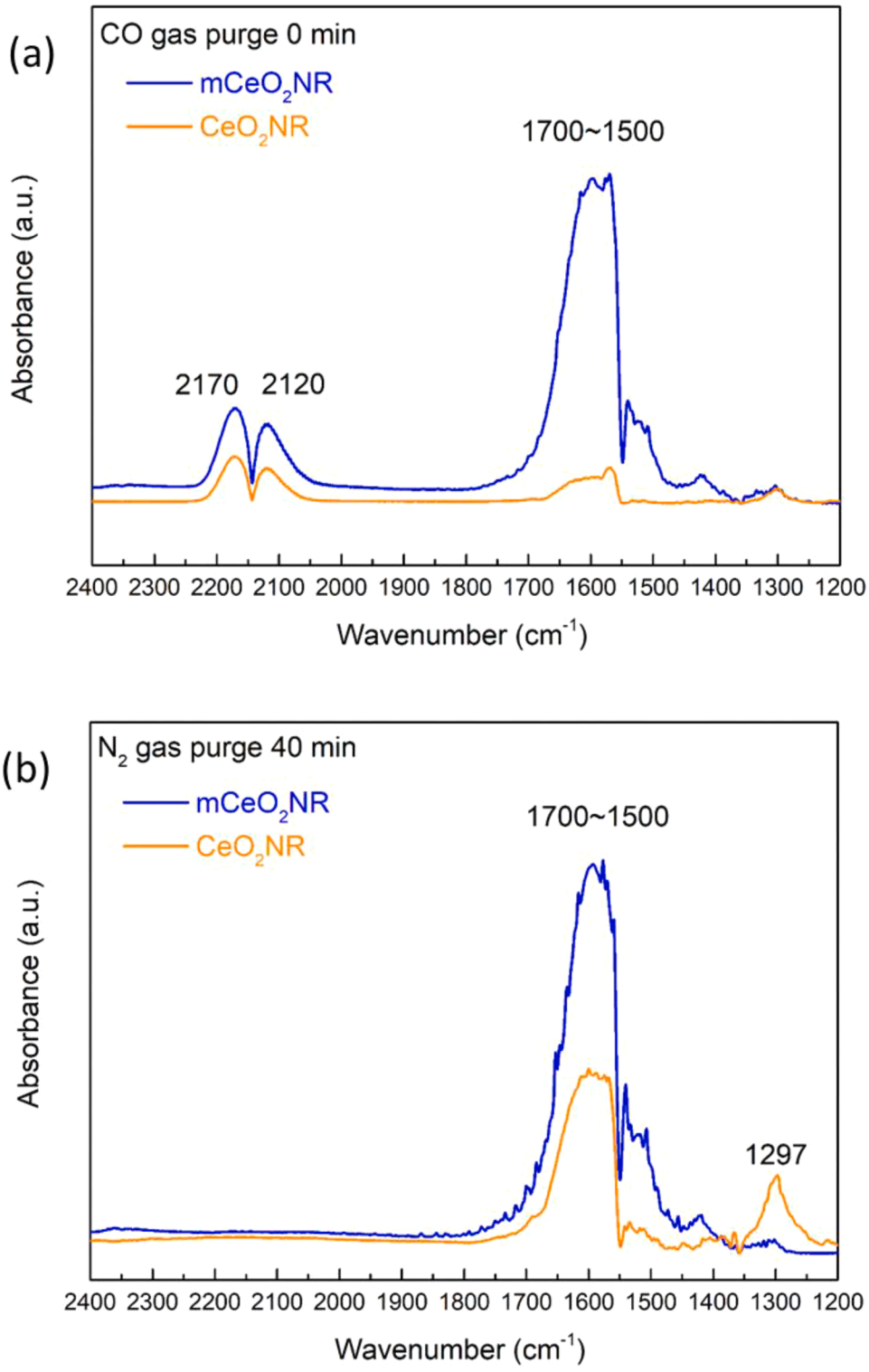

Fig. 5. *In situ* DRIFTS spectra of CO adsorption of pristine CeO_2NR and modified CeO_2NR when (a) CO gas feeding started and (b) N_2 gas feeding finished.

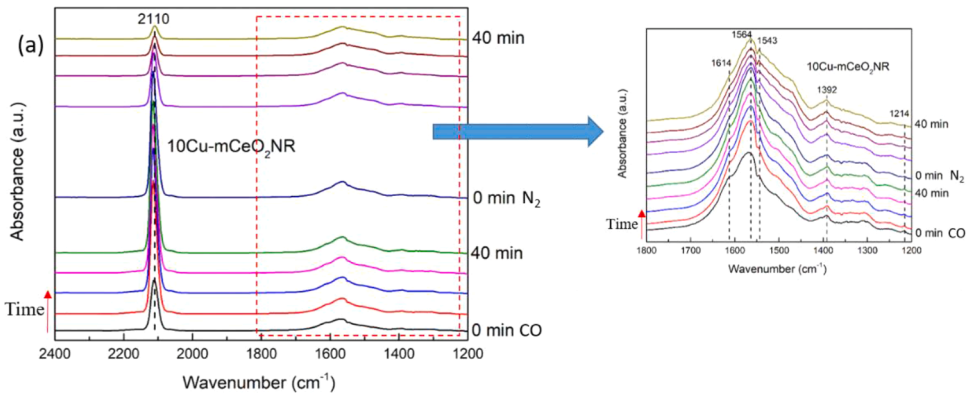

Fig. 6. *In situ* DRIFTS spectra of CO adsorption on (a) 10Cu-mCeO$_2$NR, (b) 10Ni-mCeO$_2$NR, (c) 10Co-mCeO$_2$NR, (d) 10Fe-mCeO$_2$NR, and (e) 10Mn-mCeO$_2$NR.

the system, the CO-DRIFTS data for CeO$_2$NR and mCeO$_2$NR presents that the CO adsorbed much faster and higher concentration on the surface of mCeO$_2$NR than on the surface of pristine CeO$_2$NR, indicating higher number of CO adsorption sites and easy formation of polydentate carbonate type species on mCeO$_2$NR. This is in agreement with the results of H$_2$-TPR and CO catalytic oxidation [23]. Compared to CeO$_2$NR (Fig. 5 (b)), the very weak band at *ca* 1297 cm^{-1} for mCeO$_2$NR reveals a tendency for less formation of that type of bidentate carbonate. One possible explanation for these observations is that, the NaBH$_4$ etched CeO$_2$NR with more surface defects and active sites prefers to react with CO to form polydentate carbonate, compared to the formation of bidentate carbonate.

The *in situ* CO adsorption DRIFTS spectra of 10Cu-mCeO$_2$NR, 10Ni-mCeO$_2$NR, 10Co-mCeO$_2$NR, 10Fe-mCeO$_2$NR and 10Mn-mCeO$_2$NR are presented in Fig. 6. Only the Cu catalyst sample (Fig. 6(a)) demonstrates a strong band at 2110 cm^{-1} that can be mainly assigned to linear adsorbed CO with Cu(I) [36–38], which agrees with others' work that CO is difficult to linearly adsorb to transition metal catalysts except Cu [39,40]. The presence of linearly adsorbed CO on the Cu sample explains why Cu-based catalysts demonstrate excellent low temperature CO conversion: the large amount of linearly adsorbed CO on catalysts surface can easily transfer and react with adjacent oxygen to form CO$_2$ even near room temperature.

Similar to mCeO$_2$NR, there were various adsorption peaks of carbonate species and more defined profiles were observed in the mCeO$_2$NR supported TM oxide catalysts including bicarbonate [30,41] (ν(CO$_3$) at 1615), bidentate carbonate [37,42] (ν(CO$_3$) at 1579, 1568, 1564, and 1559 cm^{-1}), monodentate carbonate [37,43,44] (ν(CO$_3$) at 1543, 1530 and 1507 cm^{-1}) and bridged carbonate [45–47] (ν(CO$_3$) at 1392, 1217 cm^{-1}).

Fig. 7 compares the *in situ* CO adsorption DRIFTS spectra of the mCeO$_2$NR supported TM oxide catalysts after 40 min of UHP N$_2$ gas flow. The order of intensity for linear adsorbed CO (2110 cm^{-1}) plus bicarbonate (~ 1615 cm^{-1}) follows: 10 Cu-mCeO$_2$NR >> 10 Ni-mCeO$_2$NR > 10 Co-mCeO$_2$NR> 10 Mn-mCeO$_2$NR> 10 Fe-mCeO$_2$NR, which is consistent with the CO-TPD results (Fig. 3). And the bands around 1579 to 1559 cm^{-1} could be assigned to bidentate carbonate, where 1543 to 1507 cm^{-1} is related to polydentate. The bands at 1392 cm^{-1} could be assigned to bridged carbonate. In addition, the order of intensity for the bridged carbonate is 10 Co-mCeO$_2$NR > 10 Mn-mCeO$_2$NR> 10 Ni-mCeO$_2$NR> 10 Fe-mCeO$_2$NR, which agrees with the results of CO oxidation performance [23]. This may indicate that the bridged carbonate at 1392 cm^{-1} is associated with the CO catalytic oxidation to CO$_2$. According to Li et al. [48], when compared with bidentate carbonate, monodentate carbonate, and inorganic carboxylate, bridged carbonate species had the lowest thermal stability, and therefore were most easily decomposed to CO$_2$. It should be noted that for 10Cu-mCeO$_2$NR, the adsorption spectrum possesses not only the strongest peak of bridged carbonate, but also the unique linear CO gas adsorption, where the latter one is believed to be the main reason for its excellent CO catalytic oxidation performance. The DRIFTS band assignments of mCeO$_2$NR supported TM catalysts are summarized in Table 3.

3.4. Stability test

The temperature at 90% CO conversion was used as a criterion for evaluating the stability of the prepared catalysts. The test temperatures for CuO$_x$-mCeO$_2$NR, NiO$_x$-mCeO$_2$NR; CoO$_x$-mCeO$_2$NR, FeO$_x$-mCeO$_2$NR, are MnO$_x$-mCeO$_2$NR were 122 °C, 243 °C, 199 °C, 364 °C, and 254 °C, respectively. The stability tests at different temperatures to obtain ~90% CO conversion of each mCeO$_2$NR supported TM oxide catalyst are presented in Fig. 8, which shows that the CO conversion for all five catalysts was nearly unchanged during the dwell time of 24 h, indicating the NaBH$_4$ etching process is an effective and stable modification method to enhance the catalyst activity and durability of CO oxidation. In addition, TEM analysis after thermal stability tests shows these catalyst powders inherit the morphology of the untreated powders, especially for the mCeO$_2$NR supports.

4. Conclusions

In this work, CeO$_2$NR were chemically etched by various contents (0.6 wt%−30 wt%) of the strong reducing agent NaBH$_4$. Compared with non-etched CeO$_2$NR, mCeO$_2$NR support exhibited superior reducibility at low temperature and lower onset temperature for hydrogen consumption. According to the surface reduction temperature and hydrogen consumption, it was determined that the optimal NaBH$_4$ concentration of chemical etching of CeO$_2$NR was ~6 wt% NaBH$_4$ addition. Transition metal oxides (TM: Cu, Co, Ni, Fe and Mn) were loaded on the 6 wt% NaBH$_4$ etched CeO$_2$NR support. And the *in situ* CO-DRIFTS results show the outstanding CO adsorption ability of mCeO$_2$NR, which is related to one strong CO adsorption mode for polydentate carbonates formation found as the result of NaBH$_4$ etching. And the existence of this poly-

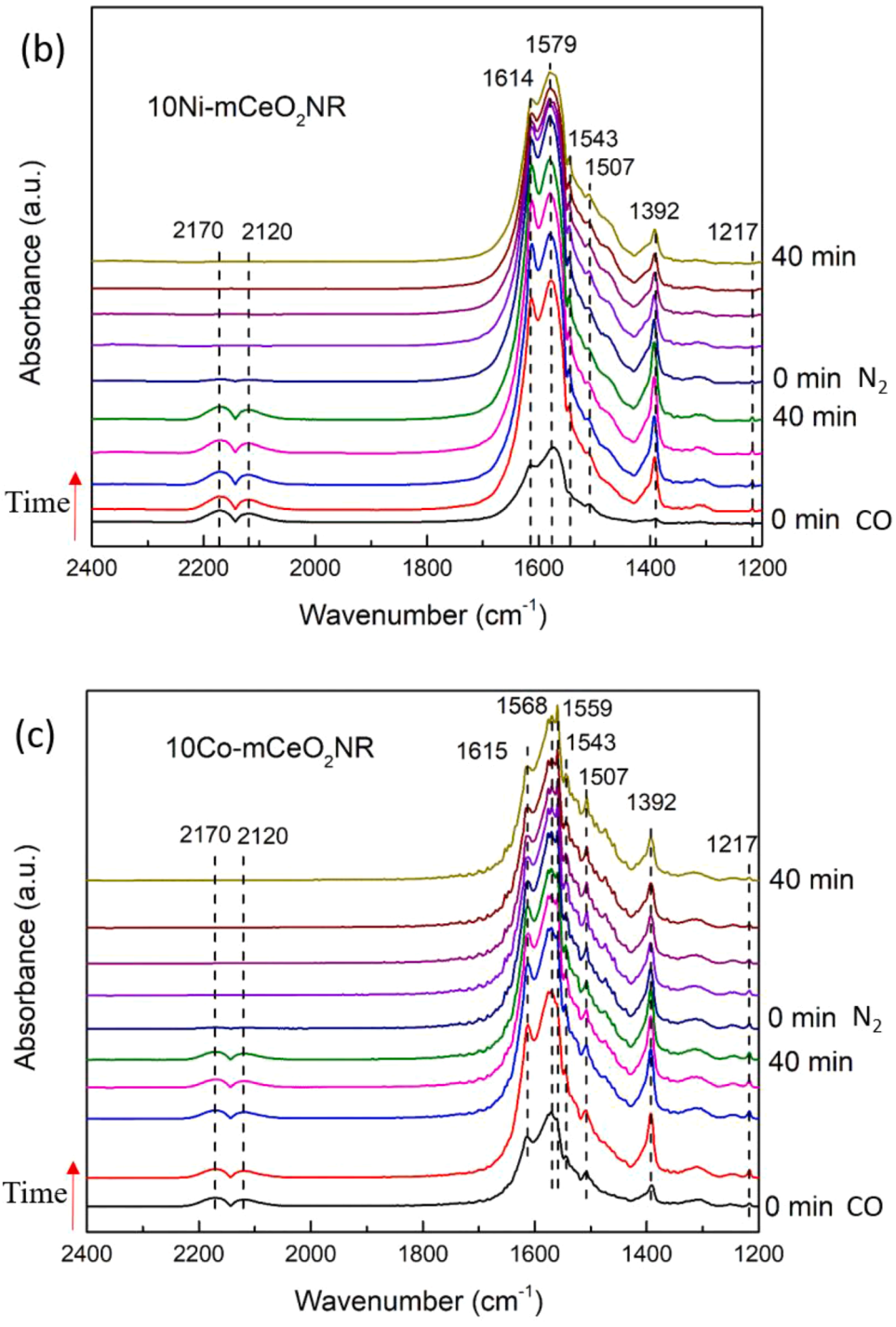

Fig. 6. (*continued*).

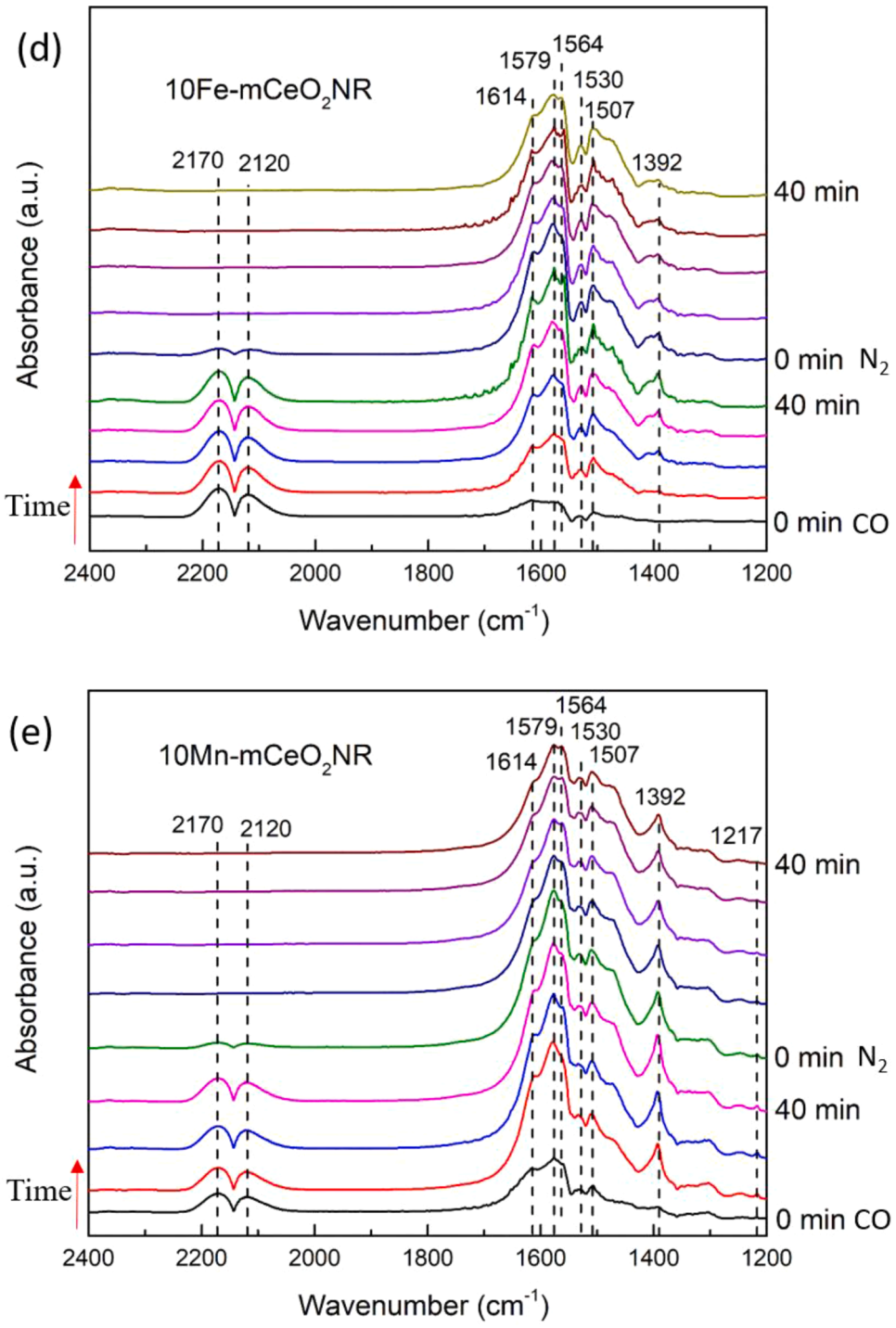

Fig. 6. (*continued*).

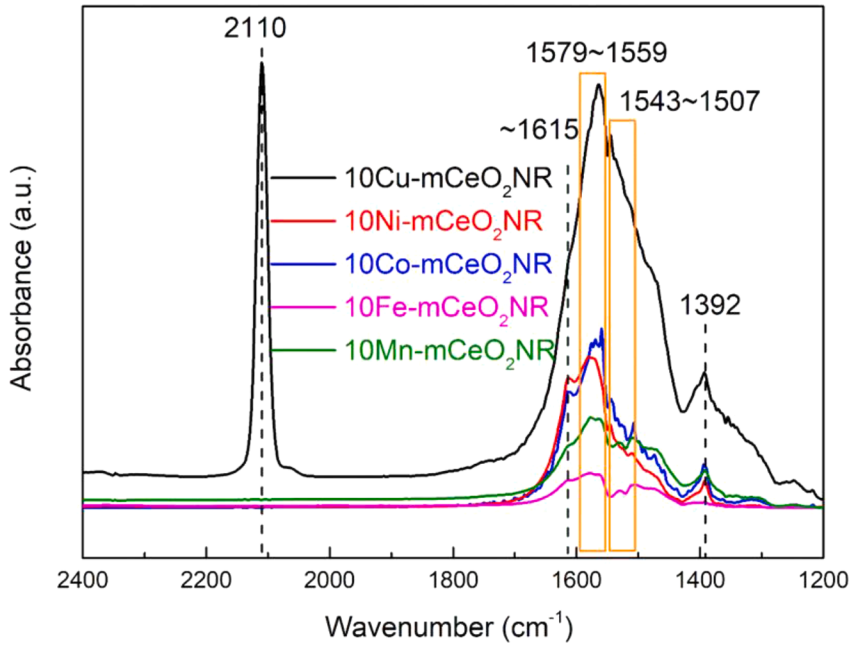

Fig. 7. *In situ* DRIFTS spectra of CO adsorption for $mCeO_2NR$ supported TM oxide catalysts.

Table 3
Peak assignments of *in situ* DRIFTS spectra for $mCeO_2NR$ supported TM catalysts.

Wavenumber (cm^{-1})	Description	Ref
2170, 2120	CO gas	[41,42]
2110	CO—Cu Cu(I)—CO	[38-40]
1615	bicarbonate	[33,43]
1579, 1568, 1564, 1559	bidentate carbonate	[39,44]
1543, 1530, 1507	mono dentate carbonate	[39,45,47]
1392, 1217	bridged carbonate	[47-49]

dentate carbonate species can also explain the effect of $NaBH_4$ etching on CeO_2NR for CO oxidation: the extra generation of surface defects including Ce^{3+} and oxygen vacancy by etching process enhances the CO adsorption at low temperature, which further accelerates the reaction of CO to CO_2. Only the Cu oxide catalyst demonstrated a linearly adsorbed CO molecule near room temperature, indicating excellent CO adsorption that can promote low temperature catalytic CO oxidation.

Credit author statement

Yifan Wang: Investigation, Methodology, Formal analysis, Writing – original draft, Writing – review & editing; **Zhongqi Liu:** Formal analysis, review & editing; **Matthew P. Confer**: Formal analysis, review & editing; **Junhao Li:** Formal analysis, review & editing. **Ruigang Wang:** Conceptualization, Investigation, Methodology, Supervision, Formal analysis, Writing – review & editing, Funding acquisition.

Declaration of Competing Interest

The authors declare that they have no known competing financial interests or personal relationships that could have appeared to influence the work reported in this paper.

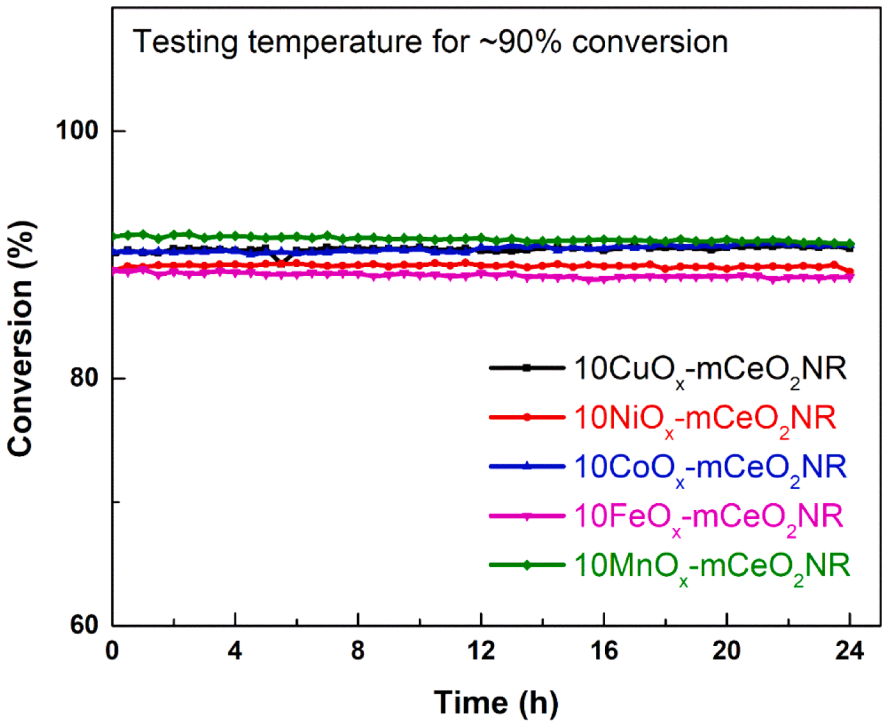

Fig. 8. Stability test for mCeO$_2$NR supported TM oxide catalysts (The test temperatures for CuO$_x$-mCeO$_2$: 122 °C; NiO$_x$-mCeO$_2$: 243 °C; CoO$_x$-mCeO$_2$: 199 °C; FeO$_x$-mCeO$_2$: 364 °C; MnO$_x$-mCeO$_2$: 254 °C).

Acknowledgement

This work is supported by National Science Foundation (CBET 1856729 and IIP-2044733). The use of TEM facilities at the Alabama Analytical Research Center (AARC) of The University of Alabama is gratefully acknowledged. The authors also gratefully acknowledge the University of Alabama College of Engineering and College of Arts and Sciences' shared analytical facility for providing the use of a Fourier transform infrared spectrometer.

Supplementary materials

Supplementary material associated with this article can be found, in the online version, at doi:10.1016/j.mcat.2021.111629.

References

[1] S. Zeng, X. Bai, X. Wang, W. Yu, Y. Liu, Valence state of active copper in CuOx/CeO$_2$ catalysts for CO oxidation, J. Rare Earths 24 (2) (2006) 177–181.
[2] S. Mahammadunnisa, P. Manoj Kumar Reddy, N. Lingaiah, C. Subrahmanyam, NiO/Ce1−xNixO$_2$−δ as an alternative to noble metal catalysts for CO oxidation, Catal. Sci. Technol. 3 (3) (2013) 730–736.
[3] B. Zhao, Z. Yang, R. Ran, Z. Guo, X. Wu, D. Weng, Fabrication of hollow-structured FeOx-MnOx oxidative catalysts with ultra-large surface area, Catal. Commun. 104 (2018) 13–16.
[4] K. Frey, V. Iablokov, G. Sáfrán, J. Osán, I. Sajó, R. Szukiewicz, S. Chenakin, N. Kruse, Nanostructured MnOx as highly active catalyst for CO oxidation, J. Catal. 287 (2012) 30–36.
[5] S.A. Mock, S.E. Sharp, T.R. Stoner, M.J. Radetic, E.T. Zell, R. Wang, CeO$_2$ nanorods-supported transition metal catalysts for CO oxidation, J. Colloid Interface Sci. 466 (2016) 261–267.
[6] R.-x. Zhou, T.-m. Yu, X.-y. Jiang, F. Chen, X.-m. Zheng, Temperature-programmed reduction and temperature-programmed desorption studies of CuO/ZrO$_2$ catalysts, Appl. Surf. Sci. 148 (3) (1999) 263–270.
[7] M.-F. Luo, P. Fang, M. He, Y.-L. Xie, In situ XRD, Raman, and TPR studies of CuO/Al$_2$O$_3$ catalysts for CO oxidation, J. Mol. Catal. A Chem. 239 (1) (2005) 243–248.
[8] C. Tang, J. Li, X. Yao, J. Sun, Y. Cao, L. Zhang, F. Gao, Y. Deng, L. Dong, Mesoporous NiO–CeO$_2$ catalysts for CO oxidation: nickel content effect and mechanism aspect, Appl. Catal. A 494 (2015) 77–86.
[9] S.T. Hossain, E. Azeeva, K. Zhang, E.T. Zell, D.T. Bernard, S. Balaz, R. Wang, A comparative study of CO oxidation over Cu-O-Ce solid solutions and CuO/CeO$_2$ nanorods catalysts, Appl. Surf. Sci. 455 (2018) 132–143.
[10] W. Blundell, G. Gowrisankaran, A. Langer, Escalation of scrutiny: the gains from dynamic enforcement of environmental regulations, Am. Econ. Rev. 110 (8) (2020) 2558–2585.
[11] X. Zheng, X. Zhang, X. Wang, S. Wang, S. Wu, Preparation and characterization of CuO/CeO$_2$ catalysts and their applications in low-temperature CO oxidation, Appl. Catal. A 295 (2) (2005) 142–149.
[12] Z. Liu, J. Li, M. Buettner, R.V. Ranganathan, M. Uddi, R. Wang, Metal–support interactions in CeO$_2$- and SiO$_2$-supported cobalt catalysts: effect of support morphology, reducibility, and interfacial configuration, ACS Appl. Mater. Interfaces 11 (18) (2019) 17035–17049.
[13] R. Wang, P.A. Crozier, R. Sharma, Structural transformation in ceria nanoparticles during redox processes, J. Phys. Chem. C 113 (14) (2009) 5700–5704.
[14] H. Huang, Q. Dai, X. Wang, Morphology effect of Ru/CeO$_2$ catalysts for the catalytic combustion of chlorobenzene, Appl. Catal. B 158-159 (2014) 96–105.
[15] Z. Liu, Y. Lu, M.P. Confer, H. Cui, J. Li, Y. Li, Y. Wang, S.C. Street, E.K. Wujcik, R. Wang, Thermally stable RuOx–CeO$_2$ nanofiber catalysts for low-temperature CO oxidation, ACS Appl. Nano Mater. 3 (8) (2020) 8403–8413.
[16] J. Li, Z. Liu, R. Wang, Support structure and reduction treatment effects on CO oxidation of SiO$_2$ nanospheres and CeO$_2$ nanorods supported ruthenium catalysts, J. Colloid Interface Sci. 531 (2018) 204–215.
[17] L. Li, L. Song, H. Wang, C. Chen, Y. She, Y. Zhan, X. Lin, Q. Zheng, Water-gas shift reaction over CuO/CeO$_2$ catalysts: effect of CeO$_2$ supports previously prepared by precipitation with different precipitants, Int. J. Hydrogen Energy 36 (15) (2011) 8839–8849.
[18] J. Li, Z. Liu, D.A. Cullen, W. Hu, J. Huang, L. Yao, Z. Peng, P. Liao, R. Wang, Distribution and valence state of Ru species on CeO$_2$ supports: support shape effect and its influence on CO oxidation, ACS Catal 9 (12) (2019) 11088–11103.
[19] Y. She, Q. Zheng, L. Li, Y. Zhan, C. Chen, Y. Zheng, X. Lin, Rare earth oxide modified CuO/CeO$_2$ catalysts for the water–gas shift reaction, Int. J. Hydrogen Energy 34 (21) (2009) 8929–8936.
[20] Y. Tanaka, T. Utaka, R. Kikuchi, T. Takeguchi, K. Sasaki, K. Eguchi, Water gas shift reaction for the reformed fuels over Cu/MnO catalysts prepared via spinel-type oxide, J. Catal. 215 (2) (2003) 271–278.
[21] W. Gao, Z. Zhang, J. Li, Y. Ma, Y. Qu, Surface engineering on CeO$_2$ nanorods by chemical redox etching and their enhanced catalytic activity for CO oxidation, Nanoscale 7 (27) (2015) 11686–11691.
[22] S. Bae, S. Gim, H. Kim, K. Hanna, Effect of NaBH$_4$ on properties of nanoscale zero-valent iron and its catalytic activity for reduction of p-nitrophenol, Appl. Catal. B 182 (2016) 541–549.
[23] Y. Wang, Z. Liu, R. Wang, NaBH$_4$ surface modification on CeO$_2$ nanorods supported transition-metal catalysts for low temperature CO oxidation, ChemCatChem 12 (17) (2020) 4304–4316.
[24] J. Lee, Y. Ryou, X. Chan, T.J. Kim, D.H. Kim, How Pt interacts with CeO$_2$ under the reducing and oxidizing environments at elevated temperature: the origin of improved thermal stability of Pt/CeO$_2$ compared to CeO$_2$, J. Phys. Chem. C 120 (45) (2016) 25870–25879.

[25] W. Song, A.S. Poyraz, Y. Meng, Z. Ren, S.-.Y. Chen, S.L. Suib, Mesoporous Co_3O_4 with controlled porosity: inverse micelle synthesis and high-performance catalytic CO oxidation at −60 °C, Chem. Mater. 26 (15) (2014) 4629–4639.
[26] C.-.W. Tang, L.-.C. Hsu, S.-.W. Yu, C.-.B. Wang, S.-.H. Chien, In situ FT-IR and TPD-MS study of carbon monoxide oxidation over a CeO_2/Co_3O_4 catalyst, Vib. Spectrosc 65 (2013) 110–115.
[27] J. Li, G. Lu, G. Wu, D. Mao, Y. Wang, Y. Guo, Promotional role of ceria on cobaltosic oxide catalyst for low-temperature CO oxidation, Catal. Sci. Technol. 2 (9) (2012) 1865–1871.
[28] H. Gao, W. Xu, H. He, X. Shi, X. Zhang, K.-i. Tanaka, DRIFTS investigation and DFT calculation of the adsorption of CO on Pt/TiO_2, Pt/CeO_2 and $FeOx/Pt/CeO_2$, Spectrochim. Acta Part A 71 (4) (2008) 1193–1198.
[29] S. Chen, T. Cao, Y. Gao, D. Li, F. Xiong, W. Huang, Probing surface structures of CeO_2, TiO_2, and Cu_2O nanocrystals with CO and CO_2 chemisorption, J. Phys. Chem. C 120 (38) (2016) 21472–21485.
[30] C. Li, Y. Sakata, T. Arai, K. Domen, K.-i. Maruya, T. Onishi, Adsorption of carbon monoxide and carbon dioxide on cerium oxide studied by Fourier-transform infrared spectroscopy. Part 2.—formation of formate species on partially reduced CeO_2 at room temperature, J. Chem. Soc. Faraday Trans. 1 F 85 (6) (1989) 1451–1461.
[31] C. Binet, A. Badri, M. Boutonnet-Kizling, J.-.C. Lavalley, FTIR study of carbon monoxide adsorption on ceria: CO carbonite dianion adsorbed species, J. Chem. Soc. Faraday Trans. 90 (7) (1994) 1023–1028.
[32] C. Li, K. Domen, K.-i. Maruya, T. Onishi, Spectroscopic identification of adsorbed species derived from adsorption and decomposition of formic acid, methanol, and formaldehyde on cerium oxide, J. Catal. 125 (2) (1990) 445–455.
[33] A. Badri, C. Binet, J.-.C. Lavalley, Surface-chlorinated ceria and chlorine-containing reduced Pd/CeO_2 catalysts. A FTIR study, J. Phys. Chem. 100 (20) (1996) 8363–8368.
[34] G.N. Vayssilov, M. Mihaylov, P.S. Petkov, K.I. Hadjiivanov, K.M. Neyman, Reassignment of the vibrational spectra of carbonates, formates, and related surface species on ceria: a combined density functional and infrared spectroscopy investigation, J. Phys. Chem. C 115 (47) (2011) 23435–23454.
[35] Z. Liu, J. Li, R. Wang, CeO_2 nanorods supported M–Co bimetallic oxides (M = Fe, Ni, Cu) for catalytic CO and C_3H_8 oxidation, J. Colloid Interface Sci. 560 (2020) 91–102.
[36] S. Sun, D. Mao, J. Yu, Z. Yang, G. Lu, Z. Ma, Low-temperature CO oxidation on CuO/CeO_2 catalysts: the significant effect of copper precursor and calcination temperature, Catal. Sci. Technol. 5 (6) (2015) 3166–3181.
[37] S. Yao, K. Mudiyanselage, W. Xu, A.C. Johnston-Peck, J.C. Hanson, T. Wu, D. Stacchiola, J.A. Rodriguez, H. Zhao, K.A. Beyer, K.W. Chapman, P.J. Chupas, A. Martínez-Arias, R. Si, T.B. Bolin, W. Liu, S.D. Senanayake, Unraveling the dynamic nature of a CuO/CeO_2 catalyst for CO oxidation in operando: a combined study of XANES (Fluorescence) and DRIFTS, ACS Catal 4 (6) (2014) 1650–1661.
[38] H. Zhu, Y. Chen, Z. Wang, W. Liu, L. Wang, Catalytic oxidation of CO over mesoporous copper-doped ceria catalysts via a facile CTAB-assisted synthesis, RSC Adv. 8 (27) (2018) 14888–14897.
[39] X.-m. Zhang, Y.-.Q. Deng, P. Tian, H.-h. Shang, J. Xu, Y.-.F. Han, Dynamic active sites over binary oxide catalysts: in situ/operando spectroscopic study of low-temperature CO oxidation over $MnOx-CeO_2$ catalysts, Appl. Catal. B 191 (2016) 179–191.
[40] L. Wang, Z. Wang, X. Cheng, M. Zhang, Y. Qin, C. Ma, In situ DRIFTS study of the NO + CO reaction on Fe–Co binary metal oxides over activated semi-coke supports, RSC Adv. 7 (13) (2017) 7695–7710.
[41] S.M. Lee, Y.H. Lee, D.H. Moon, J.Y. Ahn, D.D. Nguyen, S.W. Chang, S.S. Kim, Reaction mechanism and catalytic impact of Ni/CeO_2–x catalyst for low-temperature CO_2 methanation, Ind. Eng. Chem. Res. 58 (20) (2019) 8656–8662.
[42] P. Bera, A.L. Cámara, A. Hornés, A. Martínez-Arias, Comparative in Situ DRIFTS-MS Study of 12CO- and 13CO-TPR on CuO/CeO_2 Catalyst, J. Phys. Chem. C 113 (24) (2009) 10689–10695.
[43] R. Xu, H.C. Zeng, Dimensional control of cobalt-hydroxide-carbonate nanorods and their thermal conversion to one-dimensional arrays of Co_3O_4 Nanoparticles, J. Phys. Chem. B 107 (46) (2003) 12643–12649.
[44] F. Zhang, C. Yuan, X. Lu, L. Zhang, Q. Che, X. Zhang, Facile growth of mesoporous Co_3O_4 nanowire arrays on Ni foam for high performance electrochemical capacitors, JPS 203 (2012) 250–256.
[45] J. Jansson, M. Skoglundh, E. Fridell, P. Thormählen, A Mechanistic Study of Low Temperature CO Oxidation over Cobalt Oxide, Top. Catal. 16 (1) (2001) 385–389.
[46] J. Jansson, A.E.C. Palmqvist, E. Fridell, M. Skoglundh, L. Österlund, P. Thormählen, V Langer, On the catalytic activity of Co_3O_4 in low-temperature CO oxidation, J. Catal. 211 (2) (2002) 387–397.
[47] J.-.Y. Luo, M. Meng, X. Li, X.-.G. Li, Y.-.Q. Zha, T.-.D. Hu, Y.-.N. Xie, J. Zhang, Mesoporous Co_3O_4–CeO_2 and Pd/Co_3O_4–CeO_2 catalysts: synthesis, characterization and mechanistic study of their catalytic properties for low-temperature CO oxidation, J. Catal. 254 (2) (2008) 310–324.
[48] C. Li, Y. Sakata, T. Arai, K. Domen, K.-i. Maruya, T. Onishi, Carbon monoxide and carbon dioxide adsorption on cerium oxide studied by Fourier-transform infrared spectroscopy. Part 1.—formation of carbonate species on dehydroxylated CeO_2, at room temperature, J. Chem. Soc. Faraday Trans. 1 F 85 (4) (1989) 929–943.